Investigation of V_2O_5 and CeO_2 Nanoparticles: Synthesis, Characterization, and Application in Ammonium Removal from Aqueous Solutions

Zainab J. Abdel-Zahra
Chemistry Branch, Department of Applied Sciences, University of Technology, Baghdad, Iraq
zainab.j.abdulzahra@uotechnology.edu.iq

Rashed T. Rasheed
Chemistry Branch, Department of Applied Sciences, University of Technology, Baghdad, Iraq
rashed.t.rasheed@uotechnology.edu.iq

Muhsin Jaber Jweeg
College of Technical Engineering, Al-Farahidi University, Baghdad, Iraq
muhsin.jweeg@uoalfarahidi.edu.iq

M. N. Mohammed
Department of Mechanical Engineering, College of Engineering, Gulf University, Sanad, Bahrain
dr.mohammed.alshekhly@gulfuniversity.edu.bh

Thamer Adnan Abdullah
Chemistry Branch, Department of Applied Sciences, University of Technology, Baghdad, Iraq
thamer.a.abdullah@uotechnology.edu.iq

Mais A. Mohammed
Chemistry Branch, Department of Applied Sciences, University of Technology, Baghdad, Iraq
mais.a.mohammed@uotechnology.edu.iq

Ali O. Imarah
Department of Chemical Engineering, College of Engineering, University of Babylon, Hilla Babylon, Iraq
aliumara@uobabylon.edu.iq

Oday I. Abdullah
Department of Energy Engineering, College of Engineering, University of Baghdad, Iraq | College of Engineering, Gulf University, Sanad, Bahrain | Department of Mechanics, Al-Farabi Kazakh National University, Almaty, Kazakhstan
oday.abdullah@tuhh.de (corresponding author)

Received: 1 December 2024 | Revised: 27 December 2024 | Accepted: 10 February 2025

 DOI: https://doi.org/10.48084/etasr.9796

ABSTRACT

In this study, vanadium pentoxide (V_2O_5) and cerium dioxide (CeO_2) nanoparticles were synthesized using hydrothermal and autoclave methods, respectively. The nanoparticles underwent thermal treatment at 90 °C and 400 °C, followed by structural and compositional analysis through X-Ray Diffraction (XRD). The surface morphology was examined using field emission Scanning Electron Microscopy (SEM), while Atomic Force Microscopy (AFM) was employed to assess the nanoscale surface roughness. The Fourier

Transform Infrared Spectroscopy (FTIR) identified the functional groups, and the UV/Visible spectrometry evaluated their optical properties. The ammonium removal efficiency of the synthesized nanoparticles was also investigated. The results indicated that vanadium pentoxide exhibited the highest ammonium removal efficiency at 90 °C and 400 °C, with nanoparticles treated at 400 °C demonstrating enhanced performance compared to those treated at 90 °C.

Keywords-V_2O_5; CeO_2; nanoparticles; ammonium removal

I. INTRODUCTION

Globalization and rapid industrialization have led to significant environmental challenges, placing an increasing burden on human societies. Among these challenges, air pollution has emerged as a major global threat due to the industrial and urban expansion, negatively affecting human health [1]. Similarly, soil serves as a reservoir for pollutants originating from both organic and inorganic sources, further exacerbating environmental contamination [2].

Water pollution remains a critical concern, requiring continuous monitoring and policy evaluation. Although water covers nearly 71% of Earth's surface, only about 1% is available for human use. Ensuring access to clean drinking water is a growing challenge, aggravated by human activities that contribute to environmental contamination [3]. One major source of water pollution is synthetic dyes, widely used in textile and material dyeing industries. Due to their high stability and toxicity, even at low concentrations, these dyes pose significant risks to aquatic ecosystems and human health [4].

Nanoparticles such as CeO_2, Al_2O_3, and V_2O_5 have demonstrated excellent adsorption properties, making them highly effective for removing pollutants from water [5]. Adsorption is considered a promising method for ammonia-nitrogen removal due to its simplicity, high efficiency, and cost-effectiveness [6]. Silver (Ag) nanoparticles, for instance, have been synthesized and characterized using a low-cost chemical reduction method [7], highlighting the potential of nanotechnology in water purification.

Despite extensive research, there is a lack of accurate studies investigating the use of nanoparticles, especially V_2O_5, nH_2O, $Ce(OH)_4$, and CeO_2, for the removal of ammonium ions from aqueous solutions. This gap in knowledge serves as the primary motivation for the current study. The selection of adsorbents is crucial, as they must be abundant, cost-effective, simple to produce, and environmentally friendly [8]. In this study, the CeO_2 and V_2O_5 nanoparticles were synthesized using hydrothermal techniques. Their efficiency in removing NH_4^+ from aqueous solutions was evaluated by determining the adsorption capacity (q_t) and percentage removal (*%R*) under optimal conditions.

II. METHODOLOGY

A. Materials

The following chemicals were utilized in this study:

- Ammonium metavanadate (NH_4VO_3) (purity: 99.9%) and ammonium hydroxide (NH_4OH) (purity: 28–30%), obtained from Sigma-Aldrich.
- Nitric acid (HNO_3) (purity: 98.9%) from Alpha Chem.
- Urea (NH_2CONH_2) (purity: 98.9%) and ceric sulfate tetrahydrate ($Ce(SO_4)_2{\cdot}4H_2O$) (purity: 99.0%) from Merck.
- Cetyltrimethylammonium bromide (CTAB) (purity: 99.0%) from BDH.

B. Preparation of Vanadium Pentoxide Nanoparticles (V_2O_5 NPs)

V_2O_5 nanoparticles were synthesized using a hydrothermal reflux method [9]. The synthesis involved ammonium metavanadate (NH_4VO_3), cetyltrimethylammonium bromide (CTAB), and nitric acid (HNO_3) through the following steps:

- NH_4VO_3 (2 g, 1.704 mmol) and CTAB (0.2 g, 0.548 mmol) were dissolved in a distilled water-ethanol solution (7:3 ratio).
- HNO_3 was gradually added under continuous stirring until the pH reached 2.5.
- The solution was heated under reflux conditions for 6 hours to promote the reaction.
- The precipitate was washed multiple times with distilled water to remove impurities.
- The sample was dried at 90°C for 60 min and annealed at 400°C for 120 min.

Equations (1)-(3) describe the V_2O_5 synthesis process:

$$2NH_4VO_3 + 2HNO_3 + nH_2O \xrightarrow[CTAB]{CH_3CH_2OH} V_2O_5nH_2O + 2NH_4NO_3 + H_2O \quad (1)$$

$$V_2O_5nH_2O \xrightarrow{90\,^{\circ}C} V_2O_5.1.8H_2O + (n-1.8)H_2O \quad (2)$$

$$V_2O_5.1.8H_2O \xrightarrow{500^{\circ}C} V_2O_5 + 1.8H_2O \quad (3)$$

C. Synthesis of Cerium Dioxide Nanoparticles (CeO_2 NPs)

CeO_2 was synthesized through a hydrothermal process using an autoclave, including ceric sulfate tetrahydrate ($Ce(SO_4)_2{\cdot}4H_2O$), cetyltrimethylammonium bromide (CTAB), and urea (NH_2CONH_2). Primarily, 3 grams (7.425 mmol) of ceric sulfate tetrahydrate were dissolved along with 1 gram (16.66 mmol) of urea in 50 milliliters of distilled water. Additionally, 2 grams (5.487 mmol) of CTAB were dissolved in another 50 milliliters of distilled water. A magnetic stirrer was employed to ensure thorough mixing before transferring the solution into a Teflon-lined autoclave. The mixture underwent thermal treatment for six hours at 200 °C in a muffle furnace. Afterward, the contents were washed thoroughly three times with distilled water, followed by a purification process that included drying at 90 °C for one hour and annealing at 400

°C for 120 min. Equations (4)-(6) describe the CeO_2 synthesis process:

$$NH_2CONH_2 + 3H_2O \rightarrow 2NH_4OH + CO_2 \quad (4)$$

$$Ce(SO_4)_2.4H_2O + 4NH_4OH \rightarrow Ce(OH)_4 + 4H_2O \quad (5)$$

$$Ce(OH)_4 \xrightarrow{400°C} CeO_2 + 2H_2O \quad (6)$$

D. Adsorption of Ammonium Pollutants

The following process was employed to measure ammonium removal applying a spectrophotometer/UV method at a wavelength of 508 nm. Two 50 ml containers were prepared, one designated for the test (T) and the other for the blank (B). For each nanoparticle (V_2O_5 and CeO_2), 0.01 g was added to the T containers. Using a micropipette, 5 ml of carbonate buffer (pH = 10) was added to containers T and B. Ammonium hydroxide (0.15 ml) was then added to each container. To guarantee ideal mixing, all containers were then shaken for 15 min at 250 rpm. Then, for a 20-min incubation period, 0.25 ml of ninhydrin was added to containers T and B. A spectrophotometer was used to measure the absorbances at λ = 508 nm.

The ammonium removal percentage (*%R*) was calculated by dividing the initial concentration by the difference between the final and initial concentrations, as demonstrated in [11]:

$$\text{Percentage removal (\%R)} = \left[\frac{C_o - C_t}{C_o}\right] \times 100 \quad (7)$$

where Co is the initial ammonium concentration (mg/L) and Ct is the final ammonium concentration (mg/L).

Equation (8) was employed to determine the amount of ammonium that was adsorbed at equilibrium time (q_t) [12]:

$$q_t = (C_o - C_t)\frac{V}{W} \quad (8)$$

where: V is the volume of the ammonium solution (ml), W is the weight of the nanoparticles (g), and q_t is the adsorption capacity of ammonium.

E. Optimum Condition

Both V_2O_5 and CeO_2 were used during preparation and annealing to absorb the ammonium ion contaminant. An equal weight of 0.01 g and a volume of 5.4 ml for each nanoparticle were utilized to investigate the optimal solution for the ammonium pollution removal.

1) Effect of Nanoparticle Mass

An investigation into the effect of weight on the elimination of ammonia was developed using ninhydrin. Initially, different weights of vanadium pentoxide ($V_2O_5.nH_2O$) were prepared (0.010, 0.0150, 0.020, 0.025, 0.030 g). After the addition of 150 μM ammonia and 5 ml of buffer solution to each weight, the mixture was agitated for 15 min at 250 rpm. Centrifugation was then employed to separate the components. A total volume of 5.4 ml was inserted, and ninhydrin, with a concentration of 250 μM, was added at room temperature. A spectrophotometer was utilized to quantitatively assess the absorbance. Throughout the entire experiment, other parameters were maintained, including the reaction period (20 min), pH (10), temperature (25 °C), concentration of NH_4OH (0.1122 M), and concentration of ninhydrin (0.02245 M).

2) Effect of Ammonium Concentration

The influence of concentration variations on ammonia removal using ninhydrin was assessed. Initially, various concentrations (ranging from 25-175 μM) of ammonia were prepared. Once 0.02 g of $V_2O_5.nH_2O$ was added to 5 ml of the buffer solution, the final mixture underwent 15 min of agitation at 250 rpm. Following the centrifugation process, 250 μM ninhydrin solution was added, and the mixture was thoroughly mixed at room temperature to produce a volume of 5.4 ml for absorbance determination using a spectrophotometer. All other experimental parameters were kept constant (reaction time 20 min, pH = 10, T = 25 °C, $V_2O_5.nH_2O$= 0.02 g, and ninhydrin = 0.02245 M).

3) Shake Speed Effect

This study examined the shaking speed impact on ninhydrin-mediated ammonia elimination. After carefully weighing 0.02 g of $V_2O_5.nH_2O$, 175 μM ammonia and 5 ml buffer solution were added as additional steps. Following 15 min of shaking at a range of speeds (50, 100, 150, 200, and 250 rpm), centrifugation occurred, followed by adding 250 μM ninhydrin for thorough mixing at room temperature; absorbance measurements were then conducted using a spectrophotometer, with all other experimental parameters being kept constant throughout this study (reaction time 20 min, pH = 10, t = 25 °C, $V_2O_5.nH_2O$ = 0.02 g, ninhydrin = 0.02245, NH_4^+ = 0.1122 M).

4) Shake Time Effect

The effect of the shaking duration on ninhydrin-mediated ammonia elimination was further explored. $V_2O_5.nH_2O$ was precisely weighed at 0.02 g before adding 175 μM ammonia and 5 ml buffer solution. The resultant mixture underwent agitation for various durations, namely 5, 10, 15, 20, and 25 min at 250 rpm. The solution underwent centrifugation before adding 250 μM ninhydrin at room temperature for mixing until reaching 5.4 ml in total volume. Absorbance readings were acquired through a spectrophotometer while all other experimental parameters were strictly observed during this study (reaction time 20 min, pH = 10, T = 25 °C, $V_2O_5.nH_2O$ = 0.02 g, ninhydrin = 0.02245, NH_4^+ = 0.1122 M).

III. RESULTS AND DISCUSSION

A. Optical Characteristics of the Nanoparticle Solutions

A double-beam UV-Vis spectrophotometer (1650 PC Shimadzu) was utilized to capture the absorption spectra of the synthesized materials. The spectra, corresponding to a concentration of about 1×10^{-5} M, were generated by dissolving the nanoparticles in ethanol, covering a range from 250 nm to approximately 800 nm. The band gap is depicted in Figure 1, which is derived from a plot of the optical transmission versus wavelength curves of nanoparticles at two distinct temperatures (90 and 400 °C). The energy gap value can be determined using:

$$\text{Energy gap(eV)} = \frac{1240}{\lambda max} \quad (9)$$

The first extreme transmittance, denoted by λ_{max} in nanometers (nm), is represented by the quantity 1240, which converts nanometers to electron volts [13].

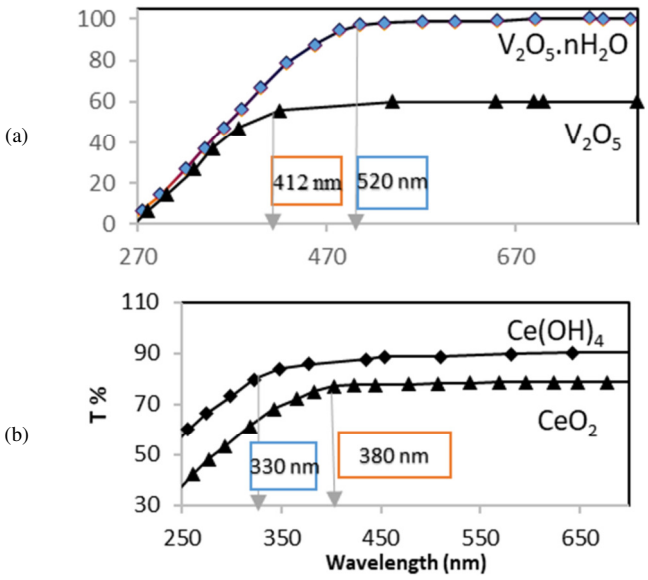

Fig. 1. The visual transmittance for nanoparticles heated at various temperatures (90 °C and 400 °C): (a) V_2O_5, (b) CeO_2.

A decrease in wavelength (blueshift) was observed in the vanadium pentoxide spectra shifting from 520 to 412 nm as the annealing temperature was increased, as illustrated in Figure 1(a). The energy gap of the synthesized $V_2O_5.nH_2O$ is 2.3 eV, while the V_2O_5 nanoparticles annealed at 400 °C, exhibiting an energy gap of 3.0 eV, which is consistent with [9]. On the other hand, the CeO_2 nanoparticles revealed that as the temperature rises, the transmittance redshifts from 330 nm to 380 nm, which is related to the transition of hydroxide $Ce(OH)_4$ to the oxide CeO_2. Consequently, the energy band of $Ce(OH)_4$ is equal to 3.7 eV (Figure 1(b)), while with the annealing of CeO_2 at 400 °C, the energy gap value is 3.2 eV, which agrees with [14].

B. Fourier Transform Infrared Spectroscopy of $V_2O_5.nH_2O$ and V_2O_5 Nanoparticles

The FTIR of both V_2O_5 nanoparticles and $V_2O_5.nH_2O$ are presented in Figure 2(a). The C=C bending vibration observed at 1406 cm^{-1} indicates the CTAB functional group. Additionally, the presence of O-H stretching and bending vibrations are noted at 3230 cm^{-1} and 1655 cm^{-1}, respectively. The V=O vibrations are characterized by peaks at 968 cm^{-1}, 731 cm^{-1}, 532 cm^{-1}, and 494 cm^{-1}. Furthermore, the stretching peak at 459 cm^{-1} explicitly confirms the presence of $V_2O_5.1.8H_2O$ nanoparticles [15-16]. Figure 2(b) portrays the characteristics of V_2O_5 after a 120-min annealing process at 400 °C. The V=O stretching vibration is detected at a wavenumber of 1020 cm^{-1}, whereas the V-O-V vibration occurs at 810 cm^{-1} [16-17]. In addition, the bands ranging from 554 to 430 cm^{-1} reveal vibrations resulted from the stretching of chain oxygen bonds [18-20].

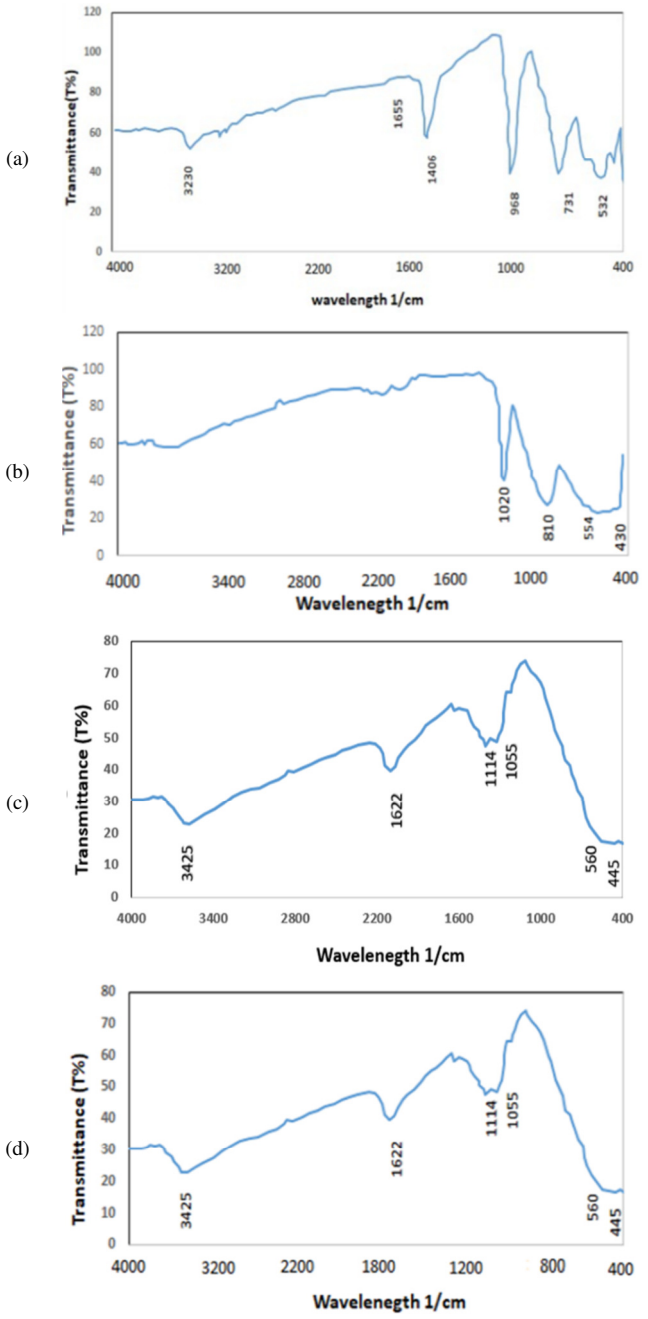

Fig. 2. FTIR analysis of: (a) V_2O_5 powder as prepared, (b) V_2O_5 powder heating at 400 °C, (c) CeO_2 powder as prepared, (d) CeO_2 powder heating at 400 °C.

C. Fourier Transform Infrared Spectroscopy for CeO_2 Nanoparticles

The FTIR spectrum of Ce(OH)4 is depicted in Figure 2(c). The molecular water molecules undergo noticeable stretching and bending vibrations, exhibited by bands at 3473 cm-1 and 1644 cm-1, respectively. A peak at 1506 cm-1 indicates the C=C bending vibration mode of CTAB, while the Ce-O and O-Ce-O stretching modes are observed at 663 cm-1 and in the range of 474 -435 cm-1, respectively. Figure 2(d) displays the

FTIR of CeO_2 after 120 min of heating at 400 °C. The stretching and bending vibrations of molecular water correspond to absorption bands between 3425 cm-1 and 1622 cm-1 [18]. The overtone bands at 1114 cm-1 are related to Ce-OH [19], while a small peak at 1055 cm-1 may indicate the presence of the C-O component that persists after annealing. Additionally, a range of 560 to 445 cm-1 is linked to the stretching mode of O-Ce-O vibration [20].

D. $V_2O_5.nH_2O$ and V_2O_5 Nanoparticle X-ray Diffraction

Figures 3(a) and 3(b) present the XRD results of the $V_2O_5.nH_2O$ and V_2O_5 nanoparticles. The primary diffraction peaks observed at 2θ values of 40.96°, 44.94°, and 47.79° are notably prominent and correspond to the (002), (411), and (600) diffraction values. These peaks are associated with $V_2O_5.nH_2O$. Additionally, the compound VOOH can be identified at an angle of 2θ = 27.8° using the JCPDS card No. 01-089-0612, associated with the card's serial number [21]. The significant diffraction peaks of 2θ values of 20.35°, 21.78°, 31.08°, 32.04°, 34.38°, 51.0°, and 61.15° are related to the five principal diffraction peaks that align with characteristic patterns associated with the V_2O_5 crystallographic planes, specifically (010), (0101), (20), (321), and (312). These peaks align with the predicted diffraction pattern of V_2O_5, as described in JCPDS card no. 41-1426. These diffraction patterns collectively indicate an orthorhombic structural arrangement for V_2O_5, with lattice constants of 11.46 Å, 3.55 Å, and 4.359 Å [22]. The derived lattice constants classify the nanocrystals within the orthorhombic system, as determined from the data presented in Table I and (10):

$$1/d^2_{hkl} = \left(\frac{h^2}{a^2} + \frac{k^2}{b^2} + \frac{l^2}{c^2}\right) \quad (10)$$

The Debye-Scherer formula, denoted as (11), is widely recognized for determining the size of crystallites by utilizing the Full Width at Half-Maximum (FWHM) intensity of diffraction peaks:

$$D = \frac{K\lambda}{\beta cos\theta} \quad (11)$$

where D is the size of the crystallite, k is the form factor (about 0.9), λ is the wavelength of X-ray (0.154 nm), and β is the FWHM intensity of an individual peak at 2θ (θ is the Bragg angle) [23].

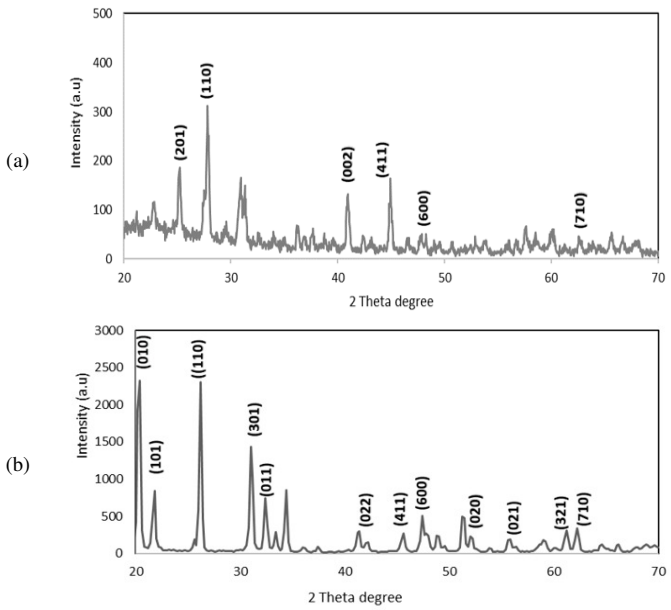

Fig. 3. (a) XRD of $V_2O_5.nH_2O$ heating at 90◦C for 60 min, (b) XRD of V_2O_5 annealing at 400 ◦C for 120 min.

TABLE I. XRD RESULTS FOR V_2O_5 AT 90 °C FOR 60 min AND 400 °C FOR 120 min

Compound	Temperature (°C)	2θ (deg)	Miller indices (hkl)	FWHM (deg)	d (Å)	D (Å)	Lattice constant (Å)		
							a	b	c
$V_2O_5.nH_2O$	90	27.88	110	0.2905	3.1974	281.66	11.42	3.34	4.40
		25.24	201	0.2889	3.5253	281.66	-	-	-
		44.94	411	0.2747	2.0152	313.80	-	-	-
V_2O_5	400	20.35	010	0.5320	4.3592	151.60	11.46	3.55	4.359
		26.21	310	0.4642	3.3964	175.60	-	-	-
		31.08	011	0.5121	2.8747	160.90	-	-	-

TABLE II. XRD RESULTS FOR CeO_2 AT 90 °C FOR 60 min AND 400 °C FOR 120 min

Compound	Temperature (°C)	2θ (deg)	hkl	FWHM (deg)	d (A°)	D (A°)	Lattice constant a=b=c (A°)
CeO_2	90	28.730	111	0.4335	2.9071	189.9	5.413
		44.229	200	0.4270	2.0461	201.0	-
		47.501	220	0.6400	1.9125	135.5	-
CeO_2	400	28.6574	111	0.7831	3.1125	104.7	5.405
		47.5430	220	0.9346	1.9110	928.3	-
		56.4018	311	0.9810	1.6300	918.0	-

E. $Ce(OH)_4$ and CeO_2 Nanoparticle X-Ray Diffraction

Figures 4(a) and 4(b) depict the X-ray data of CeO_2. A consistent pattern is exhibited with a slight variation in intensity when subjected to a temperature of 90 °C or annealed at 400 °C, suggesting the formation of CeO_2 in both scenarios. The principle peaks of $Ce(OH)_4$ at 2θ values of 28.73°, 34.50°, 47.54°, 56.49°, and 61.43° correspond to the diffractions (111), (200), (220), (311), (222), and (400) indicating a cubic structure for the CeO_2 phase [24]. To determine the size of the crystalline particles (D), Shearer's equation is applicable (10). Additionally, the lattice constants of CeO_2 nanoparticles were calculated based on Table II and (12):

$$1/d_{hkl}^2 = \frac{h^2+k^2+l^2}{a^2} \quad (12)$$

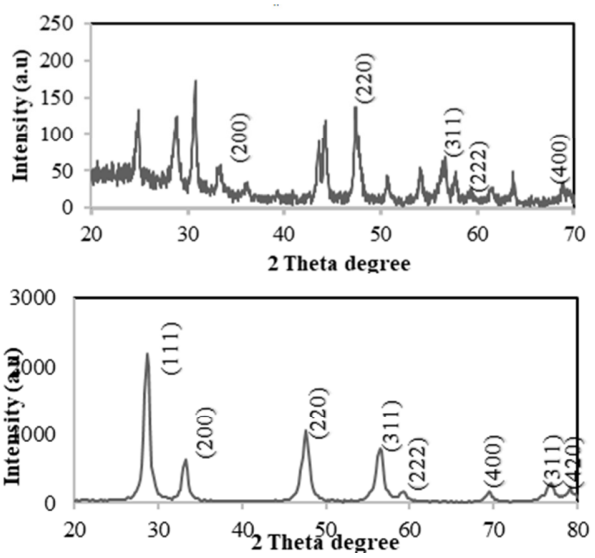

Fig. 4. XRD images of (a) $Ce(OH)_4$ heated at 90◦C for 60 min and (b) CeO_2 annealed at 400◦C for 120 min.

F. Surface Morphology by Atomic Force Microscopy of Vanadium Pnetoxide (V_2O_5) Nanoparticles

Table III illustrates the variation in the grain size of pure V_2O_5 and CeO_2 using AFM analysis. The grain size decreases from 43.15 nm of $V_2O_5.nH_2O$ to 41.07 nm of V_2O_5 as the temperature increases from 90 °C to 400 °C. This change highlights the impact of temperature on the loss of water molecules from the sample.

$$V_2O_5.nH_2O \rightarrow V_2O_5 + nH_2O \quad (13)$$

TABLE III. GRAIN SIZE VARIATION OF PURE V_2O_5 AND CeO_2 AT 90 °C AND 400 °C

Sample	Average grain size (nm)		Ionic potential (charge/radi)
	As prepared (90 °C)	Annealing (400 °C)	
V_2O_5	43.15	41.07	0.073
CeO_2	110.23	23.13	0.039

G. Surface Morphology by Atomic Force Microscopy of Cerium Dioxide (CeO_2) Nanoparticles

The initial mean particle size of Ce(OH)4 was 110.23 nm, which decreased to 23.13 nm after annealing at 400 °C, as shown in Table III. The loss of water molecules from the sample, as observed in (14), is influenced by high temperature (400 °C), which is the reason behind these observations:

$$Ce(OH)_4 \rightarrow CeO_2 + 2H_2O \quad (14)$$

H. Surface Morphology by Surface Scanning Electron Microscopy

The morphological investigation of the V_2O_5 and CeO_2 samples was conducted through Surface SEM analysis. Figure 5 illustrates the results of annealing at 400 °C for 120 min at a 400 nm enlargement. The analysis reveals a highly porous structure on the sample surface due to the rising annealing temperature. Clusters of nanoparticles interspersed with limited aggregates can be seen throughout the V_2O_5 surface morphology. Figure 5(a) appears to depict a cubic structure, whereas the SEM image of CeO_2 in Figure 5(b) suggests the presence of nanoclusters.

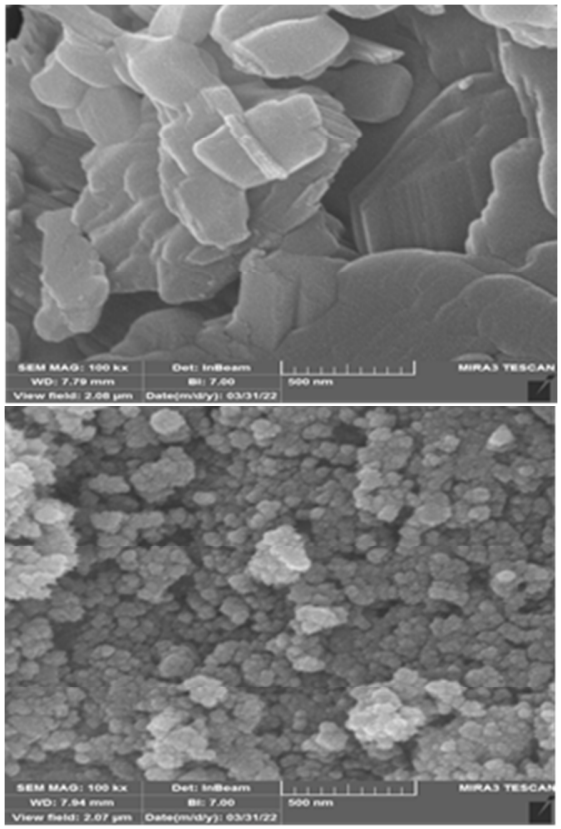

Fig. 5. SEM images of (a)V_2O_5 and (b) CeO_2 annealed at 400 °C for 120 min.

I. The Adsorption of Ammonium Pollutants onto Nanoparticles

A spectrophotometric approach was developed utilizing a wavelength of λ = 508 nm, and a yellow ninhydrin solution as an indicator. Ammonium ion (NH_4^+) and other contaminants were adsorbed from the water-based solutions using the synthesized nanoparticles in a carbonate buffer solution (50 mM, pH = 10) [22]. The percentage removal (%R) of the ammonium contaminants performed onto nanoparticles was computed by (7) for the interaction [11], while their adsorption capacity (q_t) using (8) [12].

The percentage removal (%R) of NH_4^+ from aqueous solutions varied based on two parameters: the type of nanoparticles used and the heating temperatures (90 °C and 400 °C). The finding indicated that the V_2O_5 nanoparticles presented the highest %R, and CeO_2 exhibited the lowest. As portrayed in Figure 6 and Table IV, the sequence of %R for the nanoparticles was $V_2O_5.nH_2O$ > $Ce(OH)_4$ when produced and V_2O_5 > CeO_2 after annealing. Vanadium pentoxide, as

prepared, exhibits a slight decrease in ammonium adsorption when compared to its annealed sample. This reduction is related to the increase in average grain size in the prepared state (43.15 nm), which resulted in a more significant decrease in surface area than that observed in the annealing sample (41.07 nm). The Ce(OH)4 sample, with a significantly larger surface area due to its smaller grain size (23.13 nm), enhances the adsorption of ammonium ions compared to CeO_2, as can be seen in Table III. These findings also demonstrate a consistent adsorption capacity (q_t) for the ammonium ion pollutants when subjected to heating at 90 °C, and for nanoparticles processed via the %R method and 400 °C annealing processes. This is evidenced by equal quantities and weights across all experimental iterations, as detailed in Table IV.

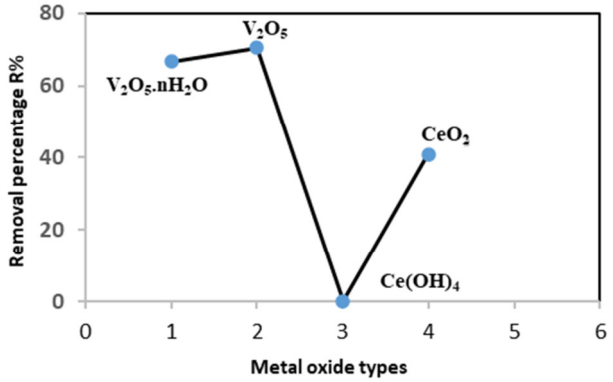

Fig. 6. Nanoparticle ammonium adsoprtion curve at 90 and 400 °C.

TABLE IV. PERCENTAGE REMOVAL (%R) AND ADSORPTION CAPACITY (Q_T) OF AMMONIUM ION POLLUTION ONTO NANOPARTICLES (HEATING AT 90 ^{O}C AND 400 ^{O}C)

Metal oxide type	Percentage removal (%R)		Adsoprtion capacity (q_t)	
	As prepared	Annealing	As prepared	Annealing
V_2O_5	66.71	70.60	7223.82	4724.2
CeO_2	0	40.93	0	1940.1

J. Optimum Condition of V2O5.nH2O to Adsorption of Ammonium Pollutants

Various parameters were examined, including the starting weight of $V_2O_5.nH_2O$ nanoparticles, concentration of ammonium ions, shaking speed, and shake time to ascertain the optimal circumstances.

1) Effect of Weight

Various weights (0.01, 0.015, 0.020, 0.025, and 0.030 g) were employed under consistent conditions: ammonium concentration fixed at 0.1122 M, ninhydrin concentration maintained at 0.02245 M, carbonate buffer concentration maintained at 0.099 M, pH held constant at 10, shake speed set to 250 rpm, and an agitation time of 15 min. Figure 7 and Table V provide comprehensive details regarding the findings.

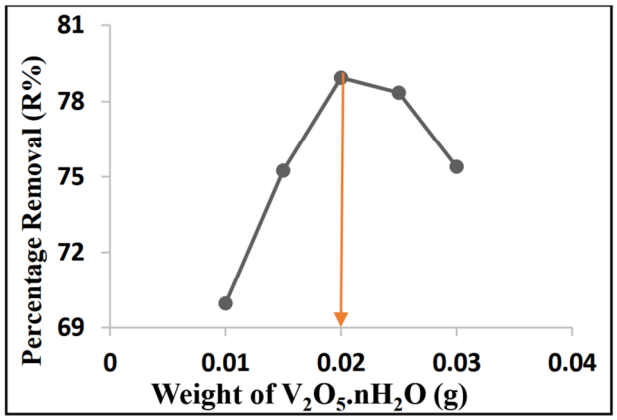

Fig. 7. Effect of adsorbent weight on ammonium removal.

TABLE V. IMPACT OF VANADIUM PENTOXIDE WEIGHT ON AMMONIUM ION POLLUTION ADSORPTION CAPACITY (QT) AND PERCENTAGE REMOVAL (%R).

Nanoparticles	Weight (g)	Percentage removal (%R)	Adsorption capacity (q_t)
$V_2O_5.nH_2O$	0.01	69.95	9160.71
	0.015	75.25	6570.00
	0.020	78.93	5168.57
	0.030	78.35	4104.00
	0.035	75.40	3291.43

The ammonium removal revealed a strong positive correlation with the increasing weight of the sorbent material. At its peak, the percentage removal equaled to 78.9% and the adsorption capacity equaled to 5198.571 when all other experimental factors remained constant. The optimal weight of the solution was 0.02 g, giving access to more adsorption sites that improved the ammonium removal efficiency.

2) Effect of Ammonium Concentration

A variety of ammonium hydroxide concentrations (2.82, 5.64, 8.64, 11.28, 14.11, 16.63, and 19.75 mg/ml) was examined against a constant $V_2O_5.nH_2O$ weight of 0.02 g. The experimental parameters included ninhydrin concentration (0.02245 M), carbonate buffer concentration (0.099 M), pH equal to 10, 250 rpm shake speed, and 15 min fixed shake time for testing. The results are illustrated in Figure 8 and Table VI. The study revealed an exponential relationship between the ammonium removal and increasing concentrations of ammonium hydroxide. The peak ammonium removal occurred at 95.704 $\%R$ and 258.402 q_t at an ammonium hydroxide concentration of 19.75 mg/ml. This finding suggests that higher ammonium hydroxide concentration provides more adsorption sites, enhancing the ammonium removal efficiency.

3) Effect of Shake Speed

Several shaking speeds were utilized to examine their effect on ammonium ion elimination (50, 100, 150, 200, and 250 rpm). In each experiment, the following variables were kept constant: pH = 10, ammonium concentration = 19.75 mg/ml, ninhydrin concentration = 0.02245 M, carbonate buffer concentration = 0.099 M, and shaking time = 15 min. Figure 9 and Table VII present the findings of this analysis. A strong positive correlation was evaluated between the ammonium removal and increasing shaking speeds, reaching its peak at

250 rpm, with maximum removal (69.23 %R and 186.923 q_t) having occurred under uniform experimental conditions. This is likely due to more readily available adsorption, which reinforces ammonium removal efficiency.

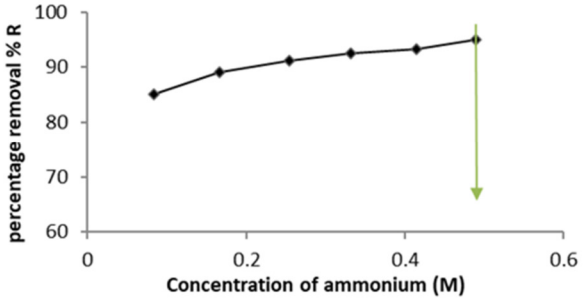

Fig. 8. Effect of concentration on ammonium elimination.

TABLE VI. THE EFFECT OF AMMONIUM CONCENTRATION ON PERCENTAGE REMOVAL (%R) AND ADSORPTION CAPACITY (QT).

Nanoparticles	Concentration (M)	Percentage removal (%R)	Adsorption capacity (q_t)
V_2O_5	0.083	85.09	229.73
	0.166	89.12	240.64
	0.254	91.27	246.42
	0.332	92.57	249.94
	0.415	93.28	251.84
	0.489	95.07	256.70

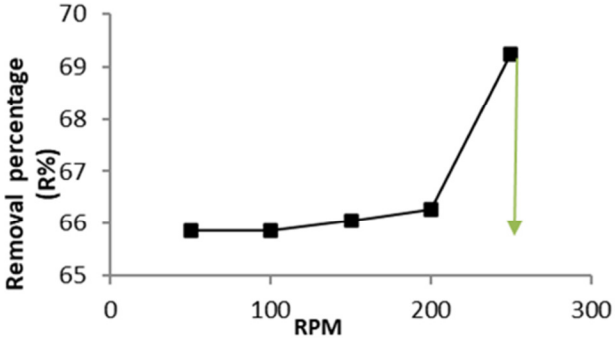

Fig. 9. Effect of shake speed on ammonium removal.

TABLE VII. SHAKING SPEED EFFECTS ON PERCENTAGE REMOVAL AND ADSORPTION CAPACITY

Nanoparticles	Shake speed (PRM)	Percentage removal (%R)	Adsorption capacity (q_t)
$V_2O_5.nH_2O$	50	65.85	177.80
	100	65.85	177.81
	150	66.06	178.36
	200	66.27	178.92
	250	69.23	186.92

4) Effect of Shake Time

The determination of how shaking duration affected ammonium elimination was estimated, using five shake intervals (5, 10, 15, 20, and 25 min) with constant values of V_2O_5.nH2O weight (0.02 g), ammonium concentration (19.75 mg/ml), ninhydrin concentration (0.2245 M), carbonate buffer concentration (0.99 M), pH = 10, and shaking speed (250 rpm). The research findings are summarized in Figure 10 and Table VIII. The removal percentage notably reduced as the shake times increased from 5 to 25 min. The highest absorption was achieved at 5min, with a removal percentage of 68.681% (q_t = 185.4).

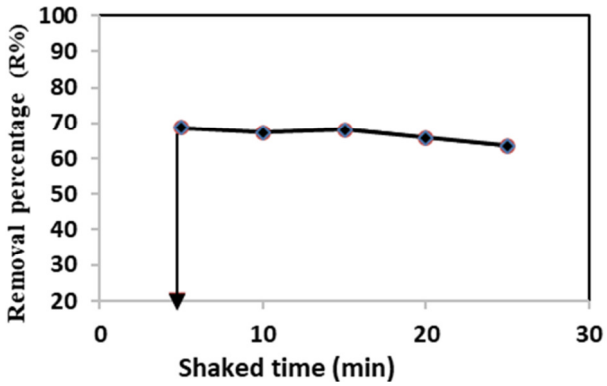

Fig. 10. Time of shake effects on ammonium elimination.

TABLE VIII. SHAKING TIME EFFECTS ON PERCENTAGE REMOVAL AND ADSORPTION CAPACITY

Nanoparticles	Shake time (min)	Percentage removal (%R)	Adsorption capacity (q_t)
$V_2O_5.nH_2O$	5	68.68	185.44
	10	67.43	182.06
	15	68.16	184.02
	20	65.87	177.84
	25	63.46	171.35

IV. CONCLUSIONS

In this study, $V_2O_5.nH_2O$, $Ce(OH)_4$, V_2O_5, and CeO_2 nanoparticles were successfully synthesized, characterized and evaluated for their effectiveness in removing ammonium ions from aqueous solutions. Unlike previous research, which did not explore the use of these nanoparticles, this study provides new insights into their adsorption capabilities. The results demonstrated that vanadium pentoxide nanoparticles exhibited the highest ammonium removal efficiency, with $V_2O_5.nH_2O$ and V_2O_5 achieving removal percentages of 66.71% and 70.60%, respectively. In contrast, $Ce(OH)_4$ and CeO_2 exhibited removal percentages of 0% and 40.93%, respectively. The lower performance of $Ce(OH)_4$ was attributed to its larger average grain size (110.23 nm), which resulted in a lower adsorption capacity.

REFERENCES

[1] H. Luo *et al.*, "Air pollution characteristics and human health risks in key cities of northwest China," *Journal of Environmental Management*, vol. 269, Sep. 2020, Art. no. 110791, https://doi.org/10.1016/j.jenvman.2020.110791.

[2] F. O. Ajibade *et al.*, "Chapter 25 - Environmental pollution and their socioeconomic impacts," in *Microbe Mediated Remediation of Environmental Contaminants*, A. Kumar, V. K. Singh, P. Singh, and V. K. Mishra, Eds. Sawston, Cambridge, UK: Woodhead Publishing, 2021, pp. 321–354.

[3] Z. A. Hassan and R. T. Rasheed, "Preparation of V2O5 and SnO2 Nanoparticles and their application as pollutant removal," *Journal of Applied Sciences and Nanotechnology*, vol. 1, no. 4, pp. 69–80, 2021.

[4] B. K. Abu Al–Roos, S. H. Lubbad, and K. K. Abu–Saqer, "Assessment of thermally treated sphagnum peat moss sorbents for removal of phenol red, bromothymol blue and malachite green from aqueous solution," *International Journal of Environmental Studies*, vol. 76, no. 5, pp. 861–872, Sep. 2019, https://doi.org/10.1080/00207233.2019.1630102.

[5] J. Saikia, A. Gogoi, and S. Baruah, "Nanotechnology for Water Remediation," in *Environmental Nanotechnology: Volume 2*, N. Dasgupta, S. Ranjan, and E. Lichtfouse, Eds. Cham, Switzerland: Springer International Publishing, 2019, pp. 195–211.

[6] P. Liang, H. Yu, J. Huang, Y. Zhang, and H. Cao, "The Review on Adsorption and Removing Ammonia Nitrogen with Biochar on its Mechanism," *MATEC Web of Conferences*, vol. 67, 2016, Art. no. 07006, https://doi.org/10.1051/matecconf/20166707006.

[7] S. Akhtar, Z. Farid, H. Ahmed, S. A. Khan, and Z. N. Khan, "Low-cost synthesis and characterization of silver nanoparticles for diverse sensing application," *Engineering, Technology & Applied Science Research*, vol. 9, no. 2, pp. 3915–3917, Apr. 2019, https://doi.org/10.48084/etasr.2450.

[8] J. Huang, N. R. Kankanamge, C. Chow, D. T. Welsh, T. Li, and P. R. Teasdale, "Removing ammonium from water and wastewater using cost-effective adsorbents: A review," *Journal of Environmental Sciences*, vol. 63, pp. 174–197, Jan. 2018, https://doi.org/10.1016/j.jes.2017.09.009.

[9] R. T. Rasheed *et al.*, "Synthesis, characterization of V2O5 nanoparticles and determination of catalase mimetic activity by new colorimetric method," *Journal of Thermal Analysis and Calorimetry*, vol. 145, no. 2, pp. 297–307, Jul. 2021, https://doi.org/10.1007/s10973-020-09725-5.

[10] T. A. Abdullah *et al.*, "V2O5, CeO2 and Their MWCNTs Nanocomposites Modified for the Removal of Kerosene from Water," *Nanomaterials*, vol. 12, no. 2, Jan. 2022, Art. no. 189, https://doi.org/10.3390/nano12020189.

[11] A. Alshameri *et al.*, "Adsorption of ammonium by different natural clay minerals: Characterization, kinetics and adsorption isotherms," *Applied Clay Science*, vol. 159, pp. 83–93, Jun. 2018, https://doi.org/10.1016/j.clay.2017.11.007.

[12] N. Bellahsen, G. Varga, N. Halyag, S. Kertész, E. Tombácz, and C. Hodúr, "Pomegranate peel as a new low-cost adsorbent for ammonium removal," *International Journal of Environmental Science and Technology*, vol. 18, no. 3, pp. 711–722, Mar. 2021, https://doi.org/10.1007/s13762-020-02863-1.

[13] Z. H. Mahmoud, "The magnetic properties of alpha phase for iron oxide NPs that prepared from its salt by novel photolysis method," *Journal of Chemical and Pharmaceutical Research*, vol. 9, no. 8, pp. 29–33, 2017.

[14] A. G. Mahabadi, A. Mirzakhani, A. Azizi, S. Chavoshi, and Sh. Khaghani, "Extracts of *Pelargonium hortorum*: A natural and efficient fluid for fast and eco-friendly biosynthesis of CeO2 nanoparticles for antioxidant and photocatalytic applications," *Inorganic Chemistry Communications*, vol. 127, May 2021, Art. no. 108553, https://doi.org/10.1016/j.inoche.2021.108553.

[15] S. Nalini, B. Selvakumar, and P. Periasamy, "Simple synthesis and characterization of V2O5 nanoparticles by microwave assisted wet chemical method," *International Journal Engineering and Manufacturing Science*, vol. 7, no. 2, pp. 411–417, 2017.

[16] Z. Li, J. Cai, P. Cizek, H. Niu, Y. Du, and T. Lin, "A self-supported, flexible, binder-free pseudo-supercapacitor electrode material with high capacitance and cycling stability from hollow, capsular polypyrrole fibers," *Journal of Materials Chemistry A*, vol. 3, no. 31, pp. 16162–16167, Jul. 2015, https://doi.org/10.1039/C5TA03585F.

[17] Y. Wu, G. Gao, and G. Wu, "Self-assembled three-dimensional hierarchical porous V2O5/graphene hybrid aerogels for supercapacitors with high energy density and long cycle life," *Journal of Materials Chemistry A*, vol. 3, no. 5, pp. 1828–1832, Jan. 2015, https://doi.org/10.1039/C4TA05537C.

[18] D. M. D. M. Prabaharan, K. Sadaiyandi, M. Mahendran, and S. Sagadevan, "Structural, Optical, Morphological and Dielectric Properties of Cerium Oxide Nanoparticles," *Materials Research*, vol. 19, pp. 478–482, Mar. 2016, https://doi.org/10.1590/1980-5373-MR-2015-0698.

[19] S. K. Kannan and M. Sundrarajan, "A Green Approach for the Synthesis of a Cerium Oxide Nanoparticle: Characterization and Antibacterial Activity," *International Journal of Nanoscience*, vol. 13, no. 03, Jun. 2014, Art. no. 1450018, https://doi.org/10.1142/S0219581X14500185.

[20] M. S. Pujar, S. M. Hunagund, V. R. Desai, S. Patil, and A. H. Sidarai, "One-step synthesis and characterizations of cerium oxide nanoparticles in an ambient temperature via Co-precipitation method," *AIP Conference Proceedings*, vol. 1942, no. 1, Apr. 2018, Art. no. 050026, https://doi.org/10.1063/1.5028657.

[21] H.-T. Fu, Z.-K. Zhang, X.-H. Yang, and X.-Z. An, "Two-Step Synthesis of V2O5 Nanosheets with High Sensing Properties toward Acetone," in *3rd Annual International Conference on Advanced Material Engineering (AME 2017)*, Shanghai, China, Apr. 2017, pp. 372–379, https://doi.org/10.2991/ame-17.2017.61.

[22] H. M. Baker and K. F. Alzboon, "Spectrophotometric determination of ammonia using ninhydrin assay and kinetic studies," *European Journal of Chemistry*, vol. 6, no. 2, pp. 135–140, Jun. 2015, https://doi.org/10.5155/eurjchem.6.2.135-140.1178.

[23] A. M. Baghdadi, A. A. Saddiq, A. Aissa, Y. Algamal, and N. M. Khalil, "Structural refinement and antimicrobial activity of aluminum oxide nanoparticles," *Journal of the Ceramic Society of Japan*, vol. 130, no. 3, pp. 257–263, 2022, https://doi.org/10.2109/jcersj2.21140.

[24] P. P. Tumkur *et al.*, "Cerium Oxide Nanoparticles: Synthesis and Characterization for Biosafe Applications," *Nanomanufacturing*, vol. 1, no. 3, pp. 176–189, Dec. 2021, https://doi.org/10.3390/nanomanufacturing1030013.